Extreme Mechanics Letters 34 (2020) 100615

Contents lists available at ScienceDirect

Extreme Mechanics Letters

journal homepage: www.elsevier.com/locate/eml

Elastic anisotropy measure for two-dimensional crystals

Ruishan Li[1], Qian Shao[1], Enlai Gao*, Ze Liu

Department of Engineering Mechanics, School of Civil Engineering, Wuhan University, Wuhan, Hubei 430072, China

ARTICLE INFO

Article history:
Received 15 October 2019
Received in revised form 23 November 2019
Accepted 24 November 2019
Available online 4 December 2019

ABSTRACT

Similar to bulk crystals, many two-dimensional crystals exhibit elastic anisotropy. However, the measures of the elastic anisotropy in two-dimensional crystals are rarely explored. In this work, we propose a two-dimensional elastic anisotropy index (A^{SU}) which is shown to be applicable for all two-dimensional crystals. Meanwhile, from the existing 'bulk' elastic anisotropy indices, we derive the specific forms of their two-dimensional counterparts. In addition, physically, A^{SU} has a clear meaning; Technically, it has a simple and explicit expression that is easy to be used in applications. Thus we suggest A^{SU} as a simple yet universal elastic anisotropy measure. Finally, an elastic anisotropy diagram is constructed for 328 two-dimensional crystals that are grouped into four crystal systems: oblique, rectangular, square, and hexagonal crystals. We find that although the lower symmetry lattices prefer to endow two-dimensional crystals with higher elastic anisotropy, the bounds of elastic anisotropy degree are lattice-independent except the highest symmetry lattice (i.e. hexagonal lattice). This work provides a fundamental metric in characterizing elastic anisotropy of two-dimensional crystals.

1. Introduction

Elastic anisotropy, referring to a difference in the elastic responses of a material upon loading along different directions, is a common and important material behaviour. Many materials, such as reinforced composites and biological tissues, exhibit anisotropic elasticity. The elastic anisotropy of these materials not only plays an essential role to fulfil the material functions, but also affects other material properties, such as phase transformations [1], indentation resistance [2], plastic deformation [3], crack propagation [4], and toughness [5]. Thus, the measure of elastic anisotropy degree is a fundamental issue in the characterizing of material properties.

In the past decades, considerable efforts have been devoted to providing a suitable elastic anisotropy index for three-dimensional (3D) materials. Zener and Siegel [6] firstly introduced a measure of anisotropy degree for cubic crystals in terms of a single parameter $A^{\text{Zener}} = 2C_{44}/(C_{11} - C_{12})$, where C_{11}, C_{12}, and C_{44} are three independent elastic constants. This index lacks universality because it is only applied to cubic crystals. Subsequently, Chung and Buessem [7] proposed an empirical index of $A^{\text{Chung}} = (G^{\text{V}} - G^{\text{R}})/(G^{\text{V}} + G^{\text{R}})$, where G^{V} and G^{R} are the Voigt and Reuss average shear moduli, respectively. And thereafter Wang and Zheng [8] introduced an index $A^{\text{Wang}} = \|\mathbf{C} - \mathbf{C}_{\text{iso}}\| / \|\mathbf{C}\|$, which was applied to measure the elastic anisotropy of hexagonal crystals. For the sake of convenience in experiments, Ledbetter and Migliori [9] adopted the ratio of the maximum and minimum shear wave velocities among all propagation directions and polarization directions as an elastic anisotropy index. In addition, the ratio of the maximum and minimum tensile stiffness is also a simple and popular index in the measuring of the elastic anisotropy of materials, but Zhao et al. [10] demonstrated that the isotropy of tensile stiffness is not a sufficient condition for the isotropy of elasticity. As an alternative, they proposed an elastic anisotropy index based on the maximum shear-extension coupling coefficient. However, all the above-mentioned indices do not account for the full tensorial nature of the elastic stiffness of a given material and neglect the contribution of the bulk part of the stiffness tensor. Considering the bulk contributions, Ranganathan and Ostoja-Starzewski [11] proposed an elastic anisotropy index $A^{\text{Ranganathan}}$ based on the difference between the Voigt and Reuss bounds on the bulk and shear moduli $A^{\text{Ranganathan}} = K^{\text{V}}/K^{\text{R}} + 5G^{\text{V}}/G^{\text{R}} - 6$, where K^{V} and K^{R} denote the Voigt and Reuss average bulk moduli, respectively. While Kube [12] argued that $A^{\text{Ranganathan}}$ is not an absolute measure of anisotropy degree, and thereby an absolute anisotropy measure $A^{\text{Kube}} = \sqrt{[\ln(K^{\text{V}}/K^{\text{R}})]^2 + 5[\ln(G^{\text{V}}/G^{\text{R}})]^2}$ for 3D materials was proposed by adopting the log-Euclidean distance between the Voigt and Reuss stiffness tensors. More recently, Fang et al. [13] introduced a new measure of anisotropy degree based on the strain/stress energy ratio $A^{\text{Fang}} = \max_{\boldsymbol{\varepsilon}}(\max_{\mathbf{R}_\varepsilon}[(\mathbf{R}_\varepsilon\boldsymbol{\varepsilon})^{\text{T}}\mathbf{C}(\mathbf{R}_\varepsilon\boldsymbol{\varepsilon})/2]/\min_{\mathbf{R}_\varepsilon}[(\mathbf{R}_\varepsilon\boldsymbol{\varepsilon})^{\text{T}}\mathbf{C}(\mathbf{R}_\varepsilon\boldsymbol{\varepsilon})/2] - 1)$. However, the above-mentioned indices are mainly proposed for 3D crystals.

* Corresponding author.
E-mail address: enlaigao@whu.edu.cn (E. Gao).

[1] These authors contributed equally.

https://doi.org/10.1016/j.eml.2019.100615
2352-4316/

Recently, two-dimensional (2D) crystals have attracted much attention because of their fascinating properties benefiting from the dimension reduction [14–20]. Many 2D crystals, such as black phosphorous, low-symmetry transitional-metal oxides and dichalcogenides, exhibit considerable elastic anisotropy [20]. In contrast to isotropic 2D crystals, anisotropic 2D crystals offer richer low-dimensional physical properties, and thus provide a fertile ground for novel applications with respect to their elastic anisotropy. The elastic anisotropy of 2D crystals not only affects their elastic properties but also closely relates to other material properties beyond the elasticity, such as phase transformations [21], and crack propagation [22]. Hence, elastic anisotropy matters for 2D crystals and calls for a good measure. However, the above-proposed measures of 'bulk' elastic anisotropy for 3D materials usually cannot be directly applied to measure the 'plane' elastic anisotropy for 2D crystals. In addition, some of the elastic anisotropy measures cannot be explicitly expressed as functions of the components of stiffness matrix (C_{ij}) and compliance matrix (S_{ij}), which calls for complex calculations and limits their wide applications. In brief, the missing of a simple yet universal elastic anisotropy index for 2D crystals limits a quantitative understanding of the mechanical behaviours of 2D crystals.

In this work, we propose a new measure (A^{SU}) to quantify the elastic anisotropy of 2D crystals, which can be applied for all 2D crystals with different crystal symmetries. Meanwhile, the existing 3D 'bulk' elastic anisotropy indices are extended to 'plane' case in 2D crystals to compare with A^{SU}, which further demonstrates the simple yet universal nature of A^{SU}. Finally, an elastic anisotropy diagram is constructed for 328 2D crystals that are grouped into four lattice systems: oblique, rectangular, square, and hexagonal lattices. We find that although low-symmetry lattices prefer to endow 2D crystals with high elastic anisotropy degree, the bounds of the elastic anisotropy degree are lattice-independent except the crystals with highest-symmetry (i.e. hexagonal lattice).

2. Theory

2.1. An elastic anisotropy measure for 2D crystals

The linear elastic constitutive relationship of a 2D crystal can be expressed as

$$\begin{bmatrix} \sigma_{11} \\ \sigma_{22} \\ \sigma_{12} \end{bmatrix} = \begin{bmatrix} C_{11} & C_{12} & C_{16} \\ C_{12} & C_{22} & C_{26} \\ C_{16} & C_{26} & C_{66} \end{bmatrix} \begin{bmatrix} \varepsilon_{11} \\ \varepsilon_{22} \\ 2\varepsilon_{12} \end{bmatrix}, \tag{1}$$

where σ_{ij} is the stress component, ε_{ij} is the strain component, and $[C_{ij}]$ is the stiffness matrix.

Similar to the bulk stress and strain defined in the 3D elasticity system [23], we define an area stress and average strain in the 2D crystal as $\sigma_p = (\sigma_{11} + \sigma_{22})/2$ and $\varepsilon_p = (\varepsilon_{11} + \varepsilon_{22})/2$, respectively. After separating out the hydrostatic part of the stress/strain tensor, the remaining part is defined as the deviatoric stress/strain, which is written as

$$\begin{aligned} s_{ij} &= \sigma_{ij} - \sigma_p \delta_{ij} \quad (i, j = 1, 2)\,, \\ e_{ij} &= \varepsilon_{ij} - \varepsilon_p \delta_{ij} \quad (i, j = 1, 2)\,, \end{aligned} \tag{2}$$

where δ_{ij} is the Kronecker delta function. Now consider a particular realization of a 2D crystal subjected to the boundary condition of a uniform displacement, $u_i = \varepsilon^0_{ij} x_j$ [24]. Voigt estimates assume that the deformation/strain of the crystal is uniform, i.e. $\varepsilon_{ij} = \varepsilon^0_{ij}$. Thus the averaged stress in the 2D crystal can be estimated by $\langle \sigma_{ij} \rangle = \bar{\omega}^{-1} \int \sigma_{ij} d\bar{\omega} = \bar{\omega}^{-1} \int C_{ij} d\bar{\omega} \varepsilon^0_{ij}$, where $\bar{\omega}$ is the in-plane area of the 2D crystal. Considering the anisotropy nature of the 2D crystal, the local stiffness tensor C_{ij} of a given 2D crystal is a function of the crystal orientation. Therefore, we assign the single crystal orientation uniformly on a circle of 2D distribution to capture anisotropic responses in all directions. Then the responses are ensembled and averaged in these orientations, and finally, one obtains an isotropic response of the 2D crystal. As we mentioned above, the two 2nd order tensors of stress and strain are divided into hydrostatic part and deviatoric part. Then the elastic relation of the ensemble averaged stress and the strain can be expressed in terms of the shear modulus G and a so-called area modulus K as

$$\langle \sigma_{ij} \rangle = 2K^{\mathrm{V}} \varepsilon^0_p \delta_{ij} + 2G^{\mathrm{V}} e^0_{ij} \quad (i, j = 1, 2)\,. \tag{3}$$

Similarly, considering a uniform traction [25] as the boundary condition imposed on a 2D crystal as $t_i = \sigma^0_{ij} n_j$, we assume a uniform stress in the crystal as suggested by Reuss. Thus the averaged strain is estimated by $\langle \varepsilon_{ij} \rangle = \bar{\omega}^{-1} \int S_{ij} d\bar{\omega} \sigma^0_{ij}$. Upon ensemble averaging on different orientations of a circle, one obtains an isotropic response as

$$\langle \varepsilon_{ij} \rangle = \frac{1}{2K^{\mathrm{R}}} \sigma^0_p \delta_{ij} + \frac{1}{2G^{\mathrm{R}}} s^0_{ij} \quad (i, j = 1, 2)\,. \tag{4}$$

The superscripts V and R represent the Voigt and Reuss averages, respectively. The above-mentioned equations lead to the ensemble averaged stiffness and compliance matrices as follows

$$\begin{aligned} \mathbf{C}^{\mathrm{V}} &= \begin{bmatrix} K^{\mathrm{V}} + G^{\mathrm{V}} & K^{\mathrm{V}} - G^{\mathrm{V}} & 0 \\ K^{\mathrm{V}} - G^{\mathrm{V}} & K^{\mathrm{V}} + G^{\mathrm{V}} & 0 \\ 0 & 0 & G^{\mathrm{V}} \end{bmatrix}, \\ \mathbf{S}^{\mathrm{R}} &= \begin{bmatrix} \frac{1}{4}\left(\frac{1}{K^{\mathrm{R}}} + \frac{1}{G^{\mathrm{R}}}\right) & \frac{1}{4}\left(\frac{1}{K^{\mathrm{R}}} - \frac{1}{G^{\mathrm{R}}}\right) & 0 \\ \frac{1}{4}\left(\frac{1}{K^{\mathrm{R}}} - \frac{1}{G^{\mathrm{R}}}\right) & \frac{1}{4}\left(\frac{1}{K^{\mathrm{R}}} + \frac{1}{G^{\mathrm{R}}}\right) & 0 \\ 0 & 0 & \frac{1}{G^{\mathrm{R}}} \end{bmatrix}. \end{aligned} \tag{5}$$

To compute the Voigt and Reuss estimated area (K^{V}, K^{R}) and shear (G^{V}, G^{R}) moduli, we denote $\mathbf{C}$ and $\mathbf{S}$ as the local stiffness and compliance matrices in the reference coordinate system, where $\mathbf{C}$ is defined in Eq. (1) and $\mathbf{S} = \mathbf{C}^{-1}$. With an arbitrary in-plane rotation θ, the local stiffness $\bar{\mathbf{C}}(\theta)$ and compliance $\bar{\mathbf{S}}(\theta)$ matrices in the new coordinate system are computed using the transformation equations. Subsequently, by ensemble averaging the local stiffness $\bar{\mathbf{C}}(\theta)$ and compliance $\bar{\mathbf{S}}(\theta)$ matrices at different orientations on a circle of 2D distributions, the Voigt estimate of the stiffness matrix $\mathbf{C}^{\mathrm{V}}$ and Reuss estimate of the compliance matrix $\mathbf{S}^{\mathrm{R}}$ are obtained (see the Supplemental Material, Sec. S1). Combining with Eq. (5), we finally obtain

$$\begin{aligned} K^{\mathrm{V}} &= \frac{C_{11} + C_{22} + 2C_{12}}{4}, \\ G^{\mathrm{V}} &= \frac{C_{11} + C_{22} - 2C_{12} + 4C_{66}}{8}, \\ K^{\mathrm{R}} &= \frac{1}{S_{11} + S_{22} + 2S_{12}}, \\ G^{\mathrm{R}} &= \frac{2}{S_{11} + S_{22} - 2S_{12} + S_{66}}. \end{aligned} \tag{6}$$

Note that, according to extreme principle of elasticity theory, the averaged moduli of any crystal always satisfy $K^{\mathrm{R}} \le K \le K^{\mathrm{V}}$ and $G^{\mathrm{R}} \le G \le G^{\mathrm{V}}$ [26]. To provide estimates to the degree of anisotropy presented in 2D crystals, a measure of the distance between $\mathbf{C}^{\mathrm{V}}/\mathbf{C}^{\mathrm{R}}$ and $\mathbf{C}^{\mathrm{R}}/\mathbf{C}^{\mathrm{R}}$ is proposed by making use of Euclidean distance $d\left(\mathbf{C}^{\mathrm{V}}/\mathbf{C}^{\mathrm{R}}, \mathbf{C}^{\mathrm{R}}/\mathbf{C}^{\mathrm{R}}\right) = \left\| \left(\mathbf{C}^{\mathrm{V}} - \mathbf{C}^{\mathrm{R}}\right)/\mathbf{C}^{\mathrm{R}} \right\|_F$, where $\|.\|_F$ denotes the Frobenius norm and $\mathbf{C}^{\mathrm{R}} = (\mathbf{S}^{\mathrm{R}})^{-1}$. The Euclidean distance d can be expressed with the area (K^{V}, K^{R}) and shear (G^{V},

G^{R}) moduli and thus the elastic anisotropy index is defined as

$$A^{\mathrm{SU}} = \left\| \left(\mathbf{C}^{\mathrm{V}} - \mathbf{C}^{\mathrm{R}}\right) / \mathbf{C}^{\mathrm{R}} \right\|_F = \sqrt{\left(\frac{K^{\mathrm{V}}}{K^{\mathrm{R}}} - 1\right)^2 + 2\left(\frac{G^{\mathrm{V}}}{G^{\mathrm{R}}} - 1\right)^2}. \quad (7)$$

The physical significance of A^{SU} is the measure of distance between the normalized averaged stiffness tensors $\mathbf{C}^{\mathrm{V}}$ and $\mathbf{C}^{\mathrm{R}}$. When the crystal is perfectly isotropic, $\mathbf{C}^{\mathrm{V}} = \mathbf{C}^{\mathrm{R}}$ and Eq. (7) has a minimum value of zero. Otherwise, Eq. (7) has a value larger than zero.

Substituting Eq. (6) into Eq. (7), we obtain the explicit expression of the elastic anisotropy index A^{SU} as the function of C_{ij} and S_{ij}

$$\begin{aligned} A^{\mathrm{SU}} = \Bigg(& \left[\frac{1}{4}\left(C_{11} + C_{22} + 2C_{12}\right)\left(S_{11} + S_{22} + 2S_{12}\right) - 1\right]^2 \\ & + 2\left[\frac{1}{16}\left(C_{11} + C_{22} - 2C_{12} + 4C_{66}\right)\right. \\ & \left.\times \left(S_{11} + S_{22} - 2S_{12} + S_{66}\right) - 1\right]^2\Bigg)^{\frac{1}{2}}. \end{aligned} \quad (8)$$

This expression makes it easy to calculate A^{SU} once obtaining the stiffness matrices of 2D crystals.

2.2. Extension of 'bulk' elastic anisotropy indices to the 'plane' cases in 2D crystals

Most of the proposed measures of 'bulk' elastic anisotropy for 3D materials cannot be directly applied as the measure of 'plane' elastic anisotropy for 2D crystals. To provide estimates to the degree of anisotropy presents in different 2D crystals, we derive the 2D forms of $A^{\mathrm{Ranganathan}}$, A^{Kube} and A^{Fang} on the basis of the work by Ranganathan and Ostoja-Starzewski [11], Kube [12], and Fang et al. [13], respectively.

We first derive the 2D form of $A^{\mathrm{Ranganathan}}$. By contracting $\mathbf{C}^{\mathrm{V}}$ and $\mathbf{S}^{\mathrm{R}}$, we obtain $C^{\mathrm{V}}_{ij} S^{\mathrm{R}}_{ij} = K^{\mathrm{V}}/K^{\mathrm{R}} + 2G^{\mathrm{V}}/G^{\mathrm{R}}$ with $i, j = 1, 2, 6$. When the crystal is perfectly isotropic, $\mathbf{C}^{\mathrm{V}} = (\mathbf{S}^{\mathrm{R}})^{-1}$ and the equation above has a minimum value of three. And if the crystal is anisotropic, it has a value larger than three. Thereby, we derive $A^{\mathrm{Ranganathan}}$ for 2D crystals as

$$A^{\mathrm{Ranganathan}} = \frac{K^{\mathrm{V}}}{K^{\mathrm{R}}} + 2\frac{G^{\mathrm{V}}}{G^{\mathrm{R}}} - 3 \geq 0. \quad (9)$$

$A^{\mathrm{Ranganathan}}$ is identically zero for isotropic crystals. It is postulated that a larger fractional difference between the Voigt and Reuss estimated area and shear moduli would indicate a stronger degree of crystal anisotropy. Thus, the extent of a 2D crystal anisotropy can be defined by the departure of $A^{\mathrm{Ranganathan}}$ from zero, accounting for both the shear and the area moduli contributions. Subsequently, we derive the 2D form of A^{Kube}, which is defined as $A^{\mathrm{Kube}} = d_L(\mathbf{C}^{\mathrm{V}}, \mathbf{C}^{\mathrm{R}}) = \left\| \ln \mathbf{C}^{\mathrm{V}} - \ln \mathbf{C}^{\mathrm{R}} \right\|_F$, where ln(.) denotes the matrix logarithm operator. By conducting Eigen-analysis on $\mathbf{C}^{\mathrm{V}}$ and $\mathbf{C}^{\mathrm{R}}$, the log-Euclidean distance d_L can be simplified and the anisotropy index is written as

$$A^{\mathrm{Kube}} = \sqrt{\left(\ln \frac{K^{\mathrm{V}}}{K^{\mathrm{R}}}\right)^2 + 2\left(\ln \frac{G^{\mathrm{V}}}{G^{\mathrm{R}}}\right)^2}. \quad (10)$$

Finally, we give the 2D form of A^{Fang}. Although the formula of

$$A^{\mathrm{Fang}} = \max_{\boldsymbol{\varepsilon}} \left(\frac{\max_{\mathbf{R}_\varepsilon} \left[\frac{1}{2}\left(\mathbf{R}_\varepsilon \boldsymbol{\varepsilon}\right)^{\mathrm{T}} \mathbf{C} \left(\mathbf{R}_\varepsilon \boldsymbol{\varepsilon}\right)\right]}{\min_{\mathbf{R}_\varepsilon} \left[\frac{1}{2}\left(\mathbf{R}_\varepsilon \boldsymbol{\varepsilon}\right)^{\mathrm{T}} \mathbf{C} \left(\mathbf{R}_\varepsilon \boldsymbol{\varepsilon}\right)\right]} - 1 \right) \quad (11)$$

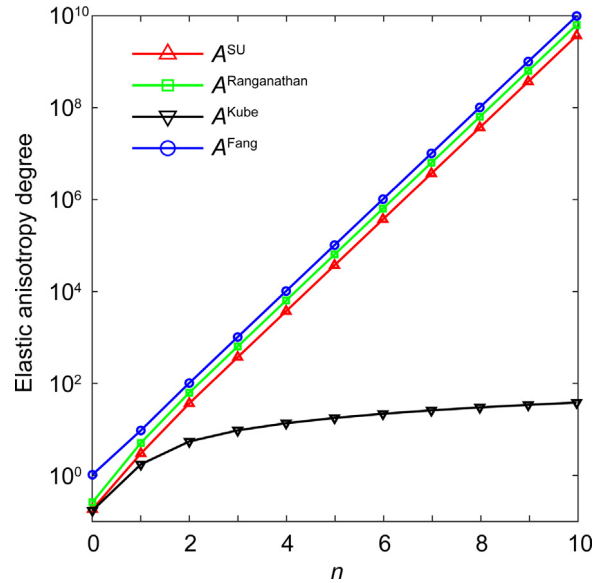

Fig. 1. A^{SU}, $A^{\mathrm{Ranganathan}}$, A^{Kube}, and A^{Fang} of 2D crystals with the increasing of condition number of the stiffness matrix.

does not change in 2D space, the strain state ($\boldsymbol{\varepsilon}$) and the rotation matrix for strain ($\mathbf{R}_\varepsilon$) are updated in the 2D form (see the Supplemental Material, Sec. S2).

Similar to A^{SU}, the anisotropy indices $A^{\mathrm{Ranganathan}}$ and A^{Kube} can also be explicitly expressed as the function of C_{ij} and S_{ij} (see the Supplemental Material, Sec. S2). But A^{Fang} has no such explicit expression. Therefore optimization algorithms are usually adopted to compute A^{Fang} [13].

2.3. Comparison of the elastic anisotropy measures for 2D crystals

To compare these elastic anisotropy indices, we calculate their values as the stiffness matrix is approaching to positive semidefinite (the condition number of following matrix increases)

$$\mathbf{C}_n = \begin{bmatrix} 2 \times 10^n & 1 & 0 \\ 1 & 2 & 0 \\ 0 & 0 & 1 \end{bmatrix} \quad (n = 0, 1, \ldots, 10). \quad (12)$$

As shown in Fig. 1, A^{SU}, $A^{\mathrm{Ranganathan}}$ and A^{Fang} exhibit similar growth trends with the increasing of n. However, the growth trend of A^{Kube} becomes slow as n increases, which originates intrinsically from the logarithmic computation in its definition. In addition, Fang et al. [13] argued that the physical meaning of $A^{\mathrm{Ranganathan}}$ is not straightforward. While the physical meaning of A^{SU} is clear, which is the measure of distance between the normalized averaged stiffness tensors $\mathbf{C}^{\mathrm{V}}$ and $\mathbf{C}^{\mathrm{R}}$. Based on the maximum strain energy ratio, the physical meaning of A^{Fang} is also clear, but A^{Fang} (Eq. (11)) cannot be explicitly expressed as a simple function of the components of stiffness matrix (C_{ij}) and compliance matrix (S_{ij}), which calls for complex computations and may limit its wide applications.

In brief, by comparison with the extension of the existing elastic anisotropy indices ($A^{\mathrm{Ranganathan}}$, A^{Kube}, and A^{Fang}), A^{SU} predicts the similar growth trend with the other two well-known measures ($A^{\mathrm{Ranganathan}}$ and A^{Fang}). Most critically, it has a clear physical meaning. Technically, A^{SU} has a simple and explicit expression that is easy to be used in engineering applications. Thus we suggest A^{SU} as a simple yet universal elastic anisotropy measure. While it should be remarked here that the extended indices A^{Kube}, $A^{\mathrm{Ranganathan}}$ and A^{Fang} can be also served as alternatives of elastic anisotropy measures for 2D crystals.

As examples, we calculate the elastic anisotropy indices of 2D crystals with different lattice systems by using the stiffness matrices of 2D crystals from first-principles calculations [27]. There are many databases of materials until now, among which JARVIS-DFT (https://jarvis.nist.gov/) is one of the most commonly used databases that organizes a variety of first principle calculated elastic tensors for a large and increasing number of 2D crystals. To date, the JARVIS-DFT contains data of computed stiffness tensors for 343 2D crystals. To avoid define the controversial thickness of 2D crystals, the elastic constants are rescaled with respect to vacuum padding, and thus the units for elastic constants are N/m. To ensure the elastic stability of crystals, the crystals with non-positive definite stiffness matrices are filtrated out from 343 2D crystals (in the numerical processing, only if the minimum eigenvalue of the stiffness matrix is larger than 0.1 N/m, the crystal is retained), which means that the rest materials satisfy the Born criteria. Afterwards, we obtain A^{SU}, $A^{Ranganathan}$, A^{Kube} and A^{Fang} for the retained 328 2D crystals (see the Supplemental Material, Table S1). The comparisons of A^{SU} with $A^{Ranganathan}$, A^{Kube} and A^{Fang} for these actual 2D crystals are shown in Fig. 2(a), which further confirm that A^{SU} exhibits similar growth trend with $A^{Ranganathan}$ and A^{Fang}. The log–log plot shown in Fig. 2(a) indicates that when the anisotropy degree is low, A^{Fang} is likely to predict a relatively larger value comparing to $A^{Ranganathan}$, A^{Kube} and A^{SU}. In addition, here we plot the distribution of A^{SU} according to statistics, from which we can find A^{SU} for 98.17% 2D crystals lie between 0 to 5 (Fig. 2(b)). We also plot the distributions of all indices and make a comparison (Fig. S1). It can be found that the anisotropy degree of many 2D crystals (77.09% for A^{SU}, 70.73% for $A^{Ranganathan}$, 74.70% for A^{Kube}, and 53.66% for A^{Fang}) is below 0.1, while only few 2D crystals exhibit very large anisotropy degree. Furthermore, because of the difference between the definitions as well as calculations of these indices, the absolute values of these indices show considerable difference. For example, the ranges of A^{SU}, $A^{Ranganathan}$, A^{Kube} and A^{Fang} for 328 2D crystals are (0.0, 39.9), (0.0, 62.9), (0.0, 5.2), and (0.0, 112.7), respectively.

3. Results and discussion

3.1. Elastic anisotropy of 2D crystals with various lattice systems

We notice that in Eq. (1), the stiffness/compliance matrix of the most general anisotropic 2D crystal has six independent constants. According to the rotational symmetry, these 2D crystals can be grouped into four lattice systems: oblique (4.27%), rectangular (31.40%), square (15.85%), and hexagonal lattices (48.48%) as shown in Fig. 3.

2D oblique crystal. If a 2D Bravais lattice has no rotational symmetry (Fig. 3(a)), its stiffness matrix is the same as in Eq. (1). Such a crystal belongs to oblique lattice system, and it has six independent elastic constants.

2D rectangular crystal. If a 2D Bravais lattice has a 2-fold rotational symmetry (Fig. 3(b)), the components C_{16} and C_{26} of its stiffness matrix take the value of zero. Such a crystal belongs to rectangular lattice system, and the number of its independent elastic constants reduces to four.

2D square crystal. If a 2D Bravais lattice has a 4-fold rotational symmetry (Fig. 3(c)), the components of its stiffness matrix would satisfy $C_{16} = C_{26} = 0$ and $C_{11} = C_{22}$. Such a crystal belongs to square lattice system, and it has three independent elastic constants, whose K^V and K^R are simplified to $K^V = K^R = (C_{11} + C_{12})/2$. And Eq. (7) is degraded into $A^{SU} = [(C_{11} - C_{12}) S_{66}/4 + (S_{11} - S_{12}) C_{66} - 1]/\sqrt{2}$.

2D hexagonal crystal. If a 2D Bravais lattice has a 6-fold rotational symmetry (Fig. 3(d)), the components of its stiffness matrix satisfy $C_{16} = C_{26} = 0$, $C_{11} = C_{22}$ and $C_{66} = (C_{11} - C_{12})/2$. Such a crystal belongs to hexagonal lattice system, and it has only two independent elastic constants. This crystal is deemed isotropic, whose K^V, K^R and G^V, G^R are simplified to $K^V = K^R = (C_{11} + C_{12})/2$ and $G^V = G^R = (C_{11} - C_{12})/2$. By using Eq. (7), zero-value of A^{SU} is found for this lattice system, suggesting its isotropic nature.

Furthermore, we extract typical 2D crystals from these four lattice systems, that are graphene (hexagonal crystal [28]), $ZnCl_2$ (square crystal), phosphorene (rectangular crystal [29]) and KCN (oblique crystal). The top and side views of their atomic structures, and the in-plane Young's and shear moduli for these four crystals are shown in Fig. 4. It can be found that the structures exhibit 6-fold, 4-fold, 2-fold and no rotational symmetry and the elastic moduli exhibit isotropic, 4-fold, 2-fold and no rotational symmetry for 2D hexagonal, square, rectangular, and oblique crystals, respectively. The A^{SU} of these four crystals are 0.00, 7.68, 0.65, and 19.30, respectively (Table 1).

3.2. Elastic anisotropy diagram for 2D crystals

We construct an elastic anisotropy diagram in the (G^V/G^R, K^V/K^R) space as shown in Fig. 5, in which we map 328 crystals from the four lattice systems. We divide the diagram into several groups by using the isolines of A^{SU} and the following information can be inferred,

(1) There is no 2D crystals in the space of ($G^V/G^R < 1$, $K^V/K^R < 1$) because of physical constraints.
(2) The crystals are elastic isotropic ($A^{SU} = 0$) in the space of ($G^V/G^R = 1$, $K^V/K^R = 1$). It can be found that all 2D hexagonal crystals lie at this point, which indicates the elastic isotropy for this crystal system.
(3) According to Eq. (7), we plot the isolines of A^{SU}. It can be found that the influence of G^V/G^R on elastic anisotropy is larger than that of K^V/K^R, and all the 2D crystals lying on the same line have equal elastic anisotropy degree. For example, $AgBiSCl_2$ and MnSe have almost equally elastic anisotropy degree ($A^{SU} \approx 0.80$).
(4) All the 2D square crystals exhibit isotropic area resistance ($K^V/K^R = 1$), hence their elastic anisotropy only depends on the shear resistance (G^V/G^R). The A^{SU} increases with the increasing of G^V/G^R. For example, AlP ($G^V/G^R = 1.806$, $A^{SU} = 1.14$) is more anisotropic than CeS ($G^V/G^R = 1.446$, $A^{SU} = 0.63$).
(5) There are a few 2D non-square crystals lying on the line of $K^V/K^R = 1$, which means that the area resistance of these crystals is also isotropic, and these crystals have similar anisotropic elasticity as 2D square crystals.
(6) The distribution of A^{SU} for 2D oblique and rectangular crystals are very scattered, indicating 2D crystals in these lattice systems prefer to have large elastic anisotropy degree. For example, AuCN ($A^{SU} = 39.99$), BPS_4 ($A^{SU} = 6.99$) and CaSn ($A^{SU} = 0.10$).
(7) For 2D oblique, rectangular and square crystals, the bounds of elastic anisotropy degree do not depend on their lattice systems.
(8) There are two crystals having K^V/K^R and G^V/G^R larger than 5, that are, BPS_4 ($K^V/K^R = 5.07$, $G^V/G^R = 5.02$, and $A^{SU} = 6.99$) and AuCN ($K^V/K^R = 8.36$, $G^V/G^R = 28.80$, and $A^{SU} = 39.99$). The atomic structures demonstrate that the atoms of these two crystals are closely packed in one direction while loosely arranged in the other perpendicular direction (Fig. S2). These considerable structural differences can help to understand their relatively large elastic anisotropy degrees.

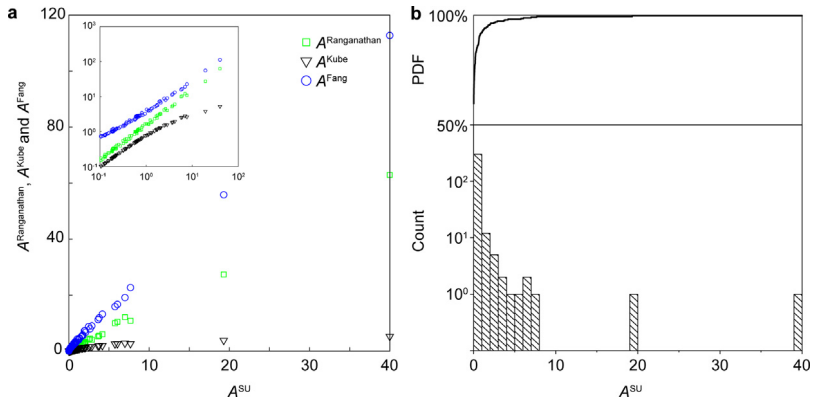

Fig. 2. (a) Comparison of A^{SU} with $A^{Ranganathan}$, A^{Kube} and A^{Fang} for crystals. Inset is the log–log plot. (b) Probability distribution function (PDF) and statistical distribution of A^{SU} for all 2D crystals.

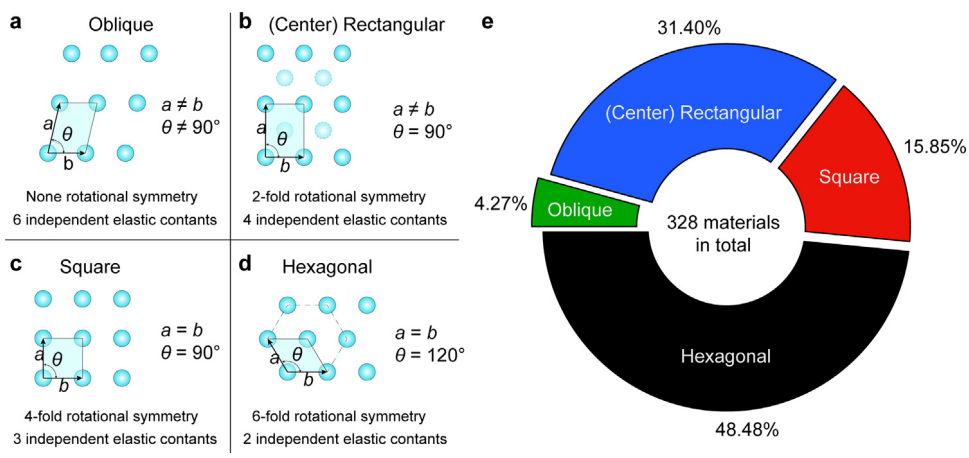

Fig. 3. (a–d) 2D Bravais lattices with different symmetries. (e) Classification and distribution of 328 2D crystals.

Table 1
Details of typical 2D crystals from four lattice systems.

JVASP-ID	Material	Lattice system	A^{SU}	$A^{Ranganathan}$	A^{Kube}	A^{Fang}	K^V/K^R	G^V/G^R
667	Graphene	Hexagonal	0.00	0.00	0.00	0.00	1.000	1.000
27773	$ZnCl_2$	Square	7.68	10.85	2.63	22.67	1.000	6.427
5983	Phosphorene	Rectangular	0.65	1.08	0.54	2.83	1.522	1.277
19996	KCN	Oblique	19.30	27.39	3.80	55.82	1.094	14.649

3.3. Additional remarks

It should be remarked here that although the elastic anisotropy of perfect 2D crystals is mainly studied, the proposed indices can be also applied to measure the elastic anisotropy of 2D crystals with defects using their elastic tensors that can be measured from experiments and computations. In addition, there are some 2D materials having pentagonal patterns. For example, Oyedele et al. [30] successfully synthesized 2D pentagonal $PdSe_2$, which exhibits intrinsic anisotropy benefiting from its unique atomic structure. The elastic anisotropy of these 2D materials can be also measured by the proposed indices from their elastic tensors that can be measured from experiments and computations.

4. Conclusion

In summary, we propose an elastic anisotropy measure (A^{SU}) for 2D crystals and extend the existing elastic anisotropy measures for 3D crystals ($A^{Ranganathan}$, A^{Kube} and A^{Fang}) into 2D configurations. The advantages and differences of A^{SU} compared with other indices are remarked herein. First, $A^{Ranganathan}$ is a relative measure of anisotropy that needs to subtract a factor to be zero-valued for the case of isotropy and lacks a clear physical meaning [12]. As a comparison, A^{SU} is defined as the measure of distance between the normalized averaged stiffness tensors $\mathbf{C}^V$ and $\mathbf{C}^R$, which has a definite physical significance. Meanwhile, due to the logarithmic computation in its definition, the growth of A^{Kube} becomes slowly when the condition number increases (Fig. 1), implying that it is insensitivity to large condition numbers, while $A^{Ranganathan}$, A^{Kube} and A^{SU} show similar growth trends. Finally, A^{SU} has a simple analytic expression compared with A^{Fang}. These combined features make A^{SU} be promising to be widely used in applications. Furthermore, the elastic anisotropy diagram offers a simple yet powerful framework to unify and map all the 328 elastic 2D crystals into a single diagram, and the elastic anisotropy form offers a systematic and concise data set of all the 2D crystals. These crystals are grouped into four lattice systems based on symmetry: oblique, rectangular, square, and hexagonal crystals. It is found that although low-symmetry lattices prefer to endow 2D crystals with high elastic anisotropy degree, the bounds of elastic anisotropy degree are lattice-independent except hexagonal lattice that has highest symmetry. This work

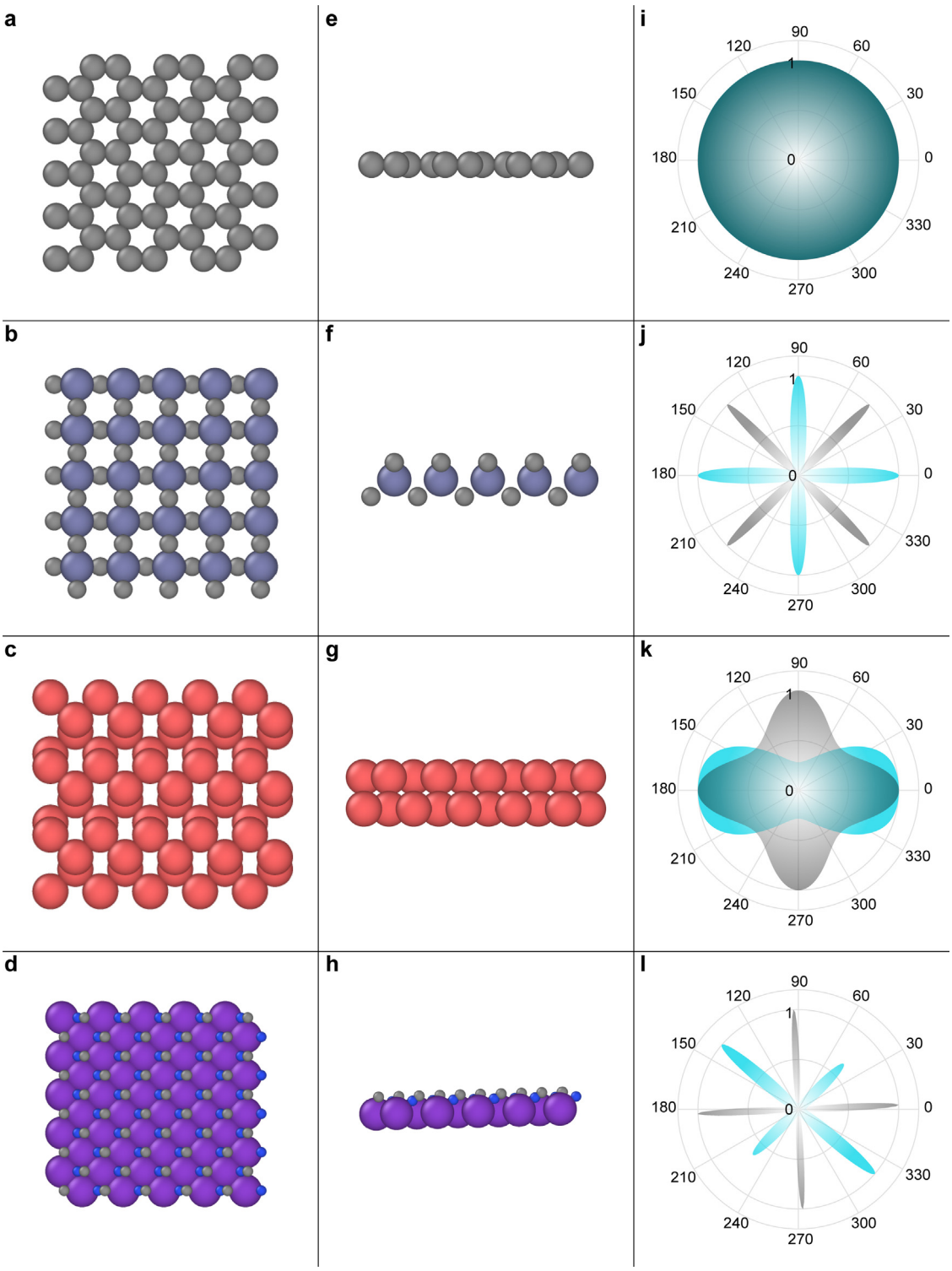

Fig. 4. Top views (a–d), and side views (e–h) of the atomic structures, and the orientation dependent in-plane Young's modulus (blue) and shear modulus (grey) (i–l) for four 2D crystals (graphene, $ZnCl_2$, phosphorene and KCN), belong to hexagonal, square, rectangular, and oblique lattice systems, respectively. The Young's and shear moduli are normalized by their maximum values in this plot.

provides a fundamental guideline in characterizing the elastic anisotropy of 2D crystals.

Declaration of competing interest

The Author declares no competing financial or non-financial interests.

Acknowledgements

This work was supported by the National Natural Science Foundation of China (11902225 and 11702199), the Natural Science Foundation of Hubei Province (2019CFB174 and 2017CFB147), and the Fundamental Research Funds for the Central Universities (413000091). The numerical calculations in this work have been

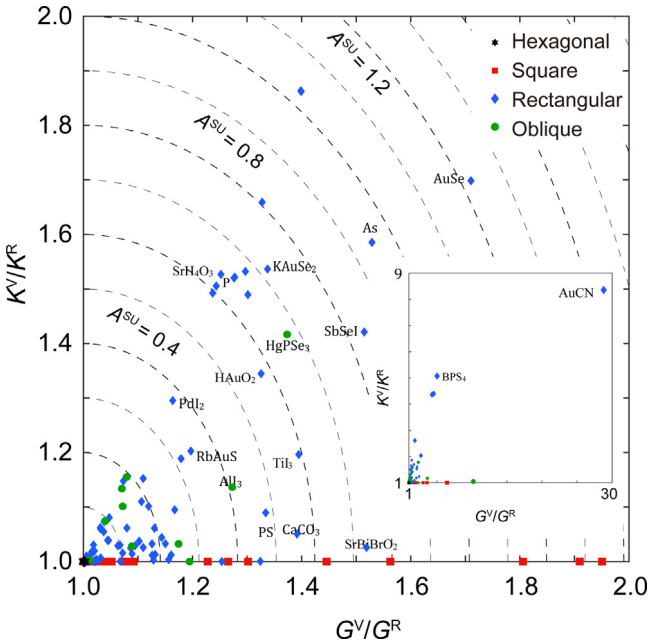

Fig. 5. Elastic anisotropy diagram for 2D crystals. Inset is the full range plot.

done on the supercomputing system in the Supercomputing Center of Wuhan University.

Appendix A. Supplementary data

Supplementary material related to this article can be found online at https://doi.org/10.1016/j.eml.2019.100615.

References

[1] M. Javanbakht, M. Adaei, Investigating the effect of elastic anisotropy on martensitic phase transformations at the nanoscale, Comput. Mater. Sci. 167 (2019) 168–182.
[2] R.S. Lakes, K. Elms, Indentability of conventional and negative Poisson's ratio foams, J. Compos. Mater. 27 (12) (2016) 1193–1202.
[3] J. Li, K.J. Van Vliet, T. Zhu, S. Yip, S. Suresh, Atomistic mechanisms governing elastic limit and incipient plasticity in crystals, Nature 418 (6895) (2002) 307–310.
[4] F. Niekiel, E. Spiecker, E. Bitzek, Influence of anisotropic elasticity on the mechanical properties of fivefold twinned nanowires, J. Mech. Phys. Solids 84 (2015) 358–379.
[5] R. Daniel, M. Meindlhumer, W. Baumegger, J. Todt, J. Zalesak, T. Ziegelwanger, C. Mitterer, J. Keckes, Anisotropy of fracture toughness in nanostructured ceramics controlled by grain boundary design, Mater. Des. 161 (2019) 80–85.
[6] C.M. Zener, S. Siegel, Elasticity and Anelasticity of Metals, University of Chicago, 1948.
[7] D.H. Chung, W.R. Buessem, The elastic anisotropy of crystals, J. Appl. Phys. 38 (5) (1967) 2010–2012.
[8] L.-F. Wang, Q.-S. Zheng, Extreme anisotropy of graphite and single-walled carbon nanotube bundles, Appl. Phys. Lett. 90 (15) (2007) 153113.
[9] H. Ledbetter, A. Migliori, A general elastic-anisotropy measure, J. Appl. Phys. 100 (6) (2006) 063516.
[10] J.-M. Zhao, X.-X. Song, B. Liu, Standardized compliance matrices for general anisotropic materials and a simple measure of anisotropy degree based on shear-extension coupling coefficient, Int. J. Appl. Mech. 08 (06) (2016) 1650076.
[11] S.I. Ranganathan, M. Ostoja-Starzewski, Universal elastic anisotropy index, Phys. Rev. Lett. 101 (5) (2008) 055504.
[12] C.M. Kube, Elastic anisotropy of crystals, AIP Adv. 6 (9) (2016) 095209.
[13] Y. Fang, Y. Wang, H. Imtiaz, B. Liu, H. Gao, Energy-ratio-based measure of elastic anisotropy, Phys. Rev. Lett. 122 (4) (2019) 045502.
[14] S.Z. Butler, S.M. Hollen, L. Cao, Y. Cui, J.A. Gupta, H.R. Gutierrez, T.F. Heinz, S.S. Hong, J. Huang, A.F. Ismach, E. Johnston-Halperin, M. Kuno, V.V. Plashnitsa, R.D. Robinson, R.S. Ruoff, S. Salahuddin, J. Shan, L. Shi, M.G. Spencer, M. Terrones, W. Windl, J.E. Goldberger, Progress, challenges, and opportunities in two-dimensional materials beyond graphene, ACS Nano 7 (4) (2013) 2898–2926.
[15] M. Heyde, S. Shaikhutdinov, H.J. Freund, Two-dimensional silica: Crystalline and vitreous, Chem. Phys. Lett. 550 (2012) 1–7.
[16] A. Splendiani, L. Sun, Y. Zhang, T. Li, J. Kim, C.Y. Chim, G. Galli, F. Wang, Emerging photoluminescence in monolayer MoS_2, Nano Lett. 10 (4) (2010) 1271–1275.
[17] Z. Zhu, D. Tomanek, Semiconducting layered blue phosphorus: A computational study, Phys. Rev. Lett. 112 (17) (2014) 176802.
[18] C. Yang, Z. Yu, P. Lu, Y. Liu, H. Ye, T. Gao, Phonon instability and ideal strength of silicene under tension, Comput. Mater. Sci. 95 (2014) 420–428.
[19] J. Yang, Y. Wang, Y. Li, H. Gao, Y. Chai, H. Yao, Edge orientations of mechanically exfoliated anisotropic two-dimensional materials, J. Mech. Phys. Solids 112 (2018) 157–168.
[20] E. Gao, Z. Xu, Thin-shell thickness of two-dimensional materials, J. Appl. Mech. 82 (2015) 121012.
[21] D. Akinwande, C.J. Brennan, J.S. Bunch, P. Egberts, J.R. Felts, H. Gao, R. Huang, J.-S. Kim, T. Li, Y. Li, K.M. Liechti, N. Lu, H.S. Park, E.J. Reed, P. Wang, B.I. Yakobson, T. Zhang, Y.-W. Zhang, Y. Zhou, Y. Zhu, A review on mechanics and mechanical properties of 2D materials—Graphene and beyond, Extreme Mech. Lett. 13 (2017) 42–77.
[22] E. Gao, S.-Z. Lin, Z. Qin, M.J. Buehler, X.-Q. Feng, Z. Xu, Mechanical exfoliation of two-dimensional materials, J. Mech. Phys. Solids 115 (2018) 248–262.
[23] W. Halliday, Fundamentals of Physics, Wiley, 1997.
[24] W. Voigt, Lehrbuch der Kristallphysik, Leipzig Teubner, 1928, p. 962.
[25] Reuss, Berechnung der Fliegrenze von Mischkristallen auf Grund der Plastizitätsbedingung für Einkristalle, J. Appl. Math. Mech. 9 (1929) 55.
[26] R. Hill, The elastic behaviour of a crystalline aggregate, Proc. Phys. Soc. Section A 65 (5) (1952) 349–354.
[27] Kamal, Dataset. http://dx.doi.org/10.6084/m9.figshare.6815705.v4, 2018.
[28] A.K. Geim, K.S. Novoselov, The rise of graphene, Nature Mater. 6 (3) (2009) 183–191.
[29] H.O. Churchill, P. Jarillo-Herrero, Two-dimensional crystals: Phosphorus joins the family, Nature Nanotechnol. 9 (5) (2014) 330–331.
[30] A.D. Oyedele, S. Yang, L. Liang, A.A. Puretzky, K. Wang, J. Zhang, P. Yu, P.R. Pudasaini, A.W. Ghosh, Z. Liu, C.M. Rouleau, B.G. Sumpter, M.F. Chisholm, W. Zhou, P.D. Rack, D.B. Geohegan, K. Xiao, PdSe2: Pentagonal two-dimensional layers with high air stability for electronics, J. Am. Chem. Soc. 139 (40) (2017) 14090–14097.

Supplemental Material

Elastic Anisotropy Measure for Two-Dimensional Crystals

Ruishan Li[a,*], Qian Shao[a,*], Enlai Gao[a,†], Ze Liu[a]

[a] *Department of Engineering Mechanics, School of Civil Engineering, Wuhan University, Wuhan, Hubei 430072, China.*

S1. Evaluation of the Voigt estimate of stiffness matrix and Reuss estimate of compliance matrix for 2D crystals

We denote $\mathbf{C}$ and $\mathbf{S}$ as the local stiffness and compliance matrices in the reference coordinate system. With an arbitrary in-plane rotation θ, the local stiffness and compliance matrices in the new coordinate system can be computed by the following transformation equations

$$\bar{\mathbf{C}}(\theta) = \mathbf{T}^{-1}\mathbf{C}\left(\mathbf{T}^{-1}\right)^{\mathrm{T}}, \tag{S1}$$

$$\bar{\mathbf{S}}(\theta) = \mathbf{T}^{\mathrm{T}}\mathbf{S}\mathbf{T}, \tag{S2}$$

where $\mathbf{T}$ is the transformation matrix defined as

$$\mathbf{T} = \begin{bmatrix} \cos^2\theta & \sin^2\theta & 2\sin\theta\cos\theta \\ \sin^2\theta & \cos^2\theta & -2\sin\theta\cos\theta \\ -\sin\theta\cos\theta & \sin\theta\cos\theta & \cos^2\theta - \sin^2\theta \end{bmatrix}. \tag{S3}$$

The Voigt estimate of the stiffness matrix and Reuss estimate of the compliance matrix can be calculated by ensemble averaging the local stiffness $\bar{\mathbf{C}}(\theta)$ and compliance $\bar{\mathbf{S}}(\theta)$ matrices at different orientations on a circle of 2D distributions as

$$C_{ij}^{\mathrm{V}} = \frac{1}{2\pi}\int_0^{2\pi} \bar{C}_{ij}(\theta)\, d\theta \quad (i, j = 1, 2, 6), \tag{S4}$$

*These authors contributed equally.

†Corresponding author. E-mail address: enlaigao@whu.edu.cn

$$S_{ij}^{\mathrm{R}} = \frac{1}{2\pi}\int_0^{2\pi} \bar{S}_{ij}\left(\theta\right) d\theta \quad (i,j=1,2,6)\,. \tag{S5}$$

Thus, each component of $\mathbf{C}^{\mathrm{V}}$ and $\mathbf{S}^{\mathrm{R}}$ is obtained

$$C_{11}^{\mathrm{V}} = C_{22}^{\mathrm{V}} = \frac{3C_{11}+3C_{22}+2C_{12}+4C_{66}}{8}, \tag{S6}$$

$$C_{12}^{\mathrm{V}} = \frac{C_{11}+C_{22}+6C_{12}-4C_{66}}{8}, \tag{S7}$$

$$C_{66}^{\mathrm{V}} = \frac{C_{11}+C_{22}-2C_{12}+4C_{66}}{8}, \tag{S8}$$

$$C_{16}^{\mathrm{V}} = C_{26}^{\mathrm{V}} = 0, \tag{S9}$$

$$S_{11}^{\mathrm{R}} = S_{22}^{\mathrm{R}} = \frac{3S_{11}+3S_{22}+2S_{12}+S_{66}}{8}, \tag{S10}$$

$$S_{12}^{\mathrm{R}} = \frac{S_{11}+S_{22}+6S_{12}-S_{66}}{8}, \tag{S11}$$

$$S_{66}^{\mathrm{R}} = \frac{S_{11}+S_{22}-2S_{12}+S_{66}}{2}, \tag{S12}$$

$$S_{16}^{\mathrm{R}} = S_{26}^{\mathrm{R}} = 0. \tag{S13}$$

S2. Extension of other elastic anisotropy indices for 2D crystals

The anisotropy index $A^{\mathrm{Ranganathan}}$ can be explicitly expressed as the function of C_{ij} and S_{ij} as follows

$$\begin{aligned} A^{\mathrm{Ranganathan}} = & \frac{1}{4}\left(C_{11}+C_{22}+2C_{12}\right)\left(S_{11}+S_{22}+2S_{12}\right) \\ & + \frac{1}{8}\left(C_{11}+C_{22}-2C_{12}+4C_{66}\right)\left(S_{11}+S_{22}-2S_{12}+S_{66}\right) - 3. \end{aligned} \tag{S14}$$

A^{Kube} measures the log-Euclidean distance between $\mathbf{C}^{\mathrm{V}}$ and $\mathbf{C}^{\mathrm{R}}$, which is

$$A^{\mathrm{Kube}} = d_L(\mathbf{C}^{\mathrm{V}}, \mathbf{C}^{\mathrm{R}}) = \left\|\ln \mathbf{C}^{\mathrm{V}} - \ln \mathbf{C}^{\mathrm{R}}\right\|_{\mathrm{F}}. \tag{S15}$$

By conducting Eigen-analysis on $\mathbf{C}^{\mathrm{V}}$ and $\mathbf{C}^{\mathrm{R}}$, one obtains

$$\mathbf{C}^{\mathrm{V}} = \mathbf{P}^{\mathrm{V}}\mathbf{\Lambda}^{\mathrm{V}}\left(\mathbf{P}^{\mathrm{V}}\right)^{-1}, \tag{S16}$$

$$\mathbf{C}^{\mathrm{R}} = \mathbf{P}^{\mathrm{R}}\mathbf{\Lambda}^{\mathrm{R}}\left(\mathbf{P}^{\mathrm{R}}\right)^{-1}, \tag{S17}$$

where $\mathbf{P}^{\mathrm{V}}$ and $\mathbf{P}^{\mathrm{R}}$ are matrices composed by eigenvectors of $\mathbf{C}^{\mathrm{V}}$ and $\mathbf{C}^{\mathrm{R}}$, respectively. $\mathbf{\Lambda}^{\mathrm{V}}$ and $\mathbf{\Lambda}^{\mathrm{R}}$ are diagonal matrices consisting of all eigenvalues of $\mathbf{C}^{\mathrm{V}}$ and $\mathbf{C}^{\mathrm{R}}$. The expressions of these matrices can be written as

$$\mathbf{P}^{\mathrm{V}} = \mathbf{P}^{\mathrm{R}} = \begin{bmatrix} 0 & 1 & 1 \\ 0 & 1 & -1 \\ 1 & 0 & 0 \end{bmatrix}, \tag{S18}$$

$$\mathbf{\Lambda}^{\mathrm{V}} = \begin{bmatrix} G^{\mathrm{V}} & 0 & 0 \\ 0 & 2K^{\mathrm{V}} & 0 \\ 0 & 0 & 2G^{\mathrm{V}} \end{bmatrix}, \tag{S19}$$

$$\mathbf{\Lambda}^{\mathrm{R}} = \begin{bmatrix} G^{\mathrm{R}} & 0 & 0 \\ 0 & 2K^{\mathrm{R}} & 0 \\ 0 & 0 & 2G^{\mathrm{R}} \end{bmatrix}. \tag{S20}$$

Based on Eqs. (S16)-(S20), the logarithms of $\mathbf{C}^{\mathrm{V}}$ and $\mathbf{C}^{\mathrm{R}}$ are derived as

$$\ln \mathbf{C}^{\mathrm{V}} = \mathbf{P}^{\mathrm{V}} \ln \mathbf{\Lambda}^{\mathrm{V}} \left(\mathbf{P}^{\mathrm{V}}\right)^{-1} = \mathbf{P}^{\mathrm{V}} \mathrm{diag}\left(\ln G^{\mathrm{V}}, \ln 2K^{\mathrm{V}}, \ln 2G^{\mathrm{V}}\right) \left(\mathbf{P}^{\mathrm{V}}\right)^{-1}, \tag{S21}$$

$$\ln \mathbf{C}^{\mathrm{R}} = \mathbf{P}^{\mathrm{R}} \ln \mathbf{\Lambda}^{\mathrm{R}} \left(\mathbf{P}^{\mathrm{R}}\right)^{-1} = \mathbf{P}^{\mathrm{R}} \mathrm{diag}\left(\ln G^{\mathrm{R}}, \ln 2K^{\mathrm{R}}, \ln 2G^{\mathrm{R}}\right) \left(\mathbf{P}^{\mathrm{R}}\right)^{-1}. \tag{S22}$$

By substituting Eqs. (S21) and (S22) into Eq. (S15), the log-Euclidean distance d_L can be simplified and then defined as the anisotropy index

$$A^{\mathrm{Kube}} = \sqrt{\left(\ln \frac{K^{\mathrm{V}}}{K^{\mathrm{R}}}\right)^2 + 2\left(\ln \frac{G^{\mathrm{V}}}{G^{\mathrm{R}}}\right)^2}. \tag{S23}$$

Similarly, using the explicit expressions of K^{V}, K^{R}, G^{V} and G^{R}, Eq. (S23) is explicitly expressed as the function of C_{ij} and S_{ij} as

$$\begin{aligned} A^{\mathrm{Kube}} = \Bigg(& \left[\ln \frac{1}{4}\left(C_{11} + C_{22} + 2C_{12}\right)\left(S_{11} + S_{22} + 2S_{12}\right)\right]^2 \\ & + 2\left[\ln \frac{1}{16}\left(C_{11} + C_{22} - 2C_{12} + 4C_{66}\right)\left(S_{11} + S_{22} - 2S_{12} + S_{66}\right)\right]^2 \Bigg)^{\frac{1}{2}}. \end{aligned} \tag{S24}$$

A^{Fang} for 2D crystals shares the same formula as in 3D space, yet the strain tensor ($\boldsymbol{\varepsilon}$) and rotation tensor for strain ($\mathbf{R}_\varepsilon$) are different in 2D form

$$\boldsymbol{\varepsilon} = \begin{bmatrix} \cos\theta \\ \sin\theta \\ 0 \end{bmatrix}, \tag{S25}$$

$$\mathbf{R}_\varepsilon = \left(\mathbf{T}^{-1}\right)^{\mathrm{T}}. \tag{S26}$$

Typically, A^{Fang} cannot be explicitly expressed as the function of C_{ij} and S_{ij}. Therefore optimization algorithms are usually adopted to compute A^{Fang}.

S3. Supplemental figures

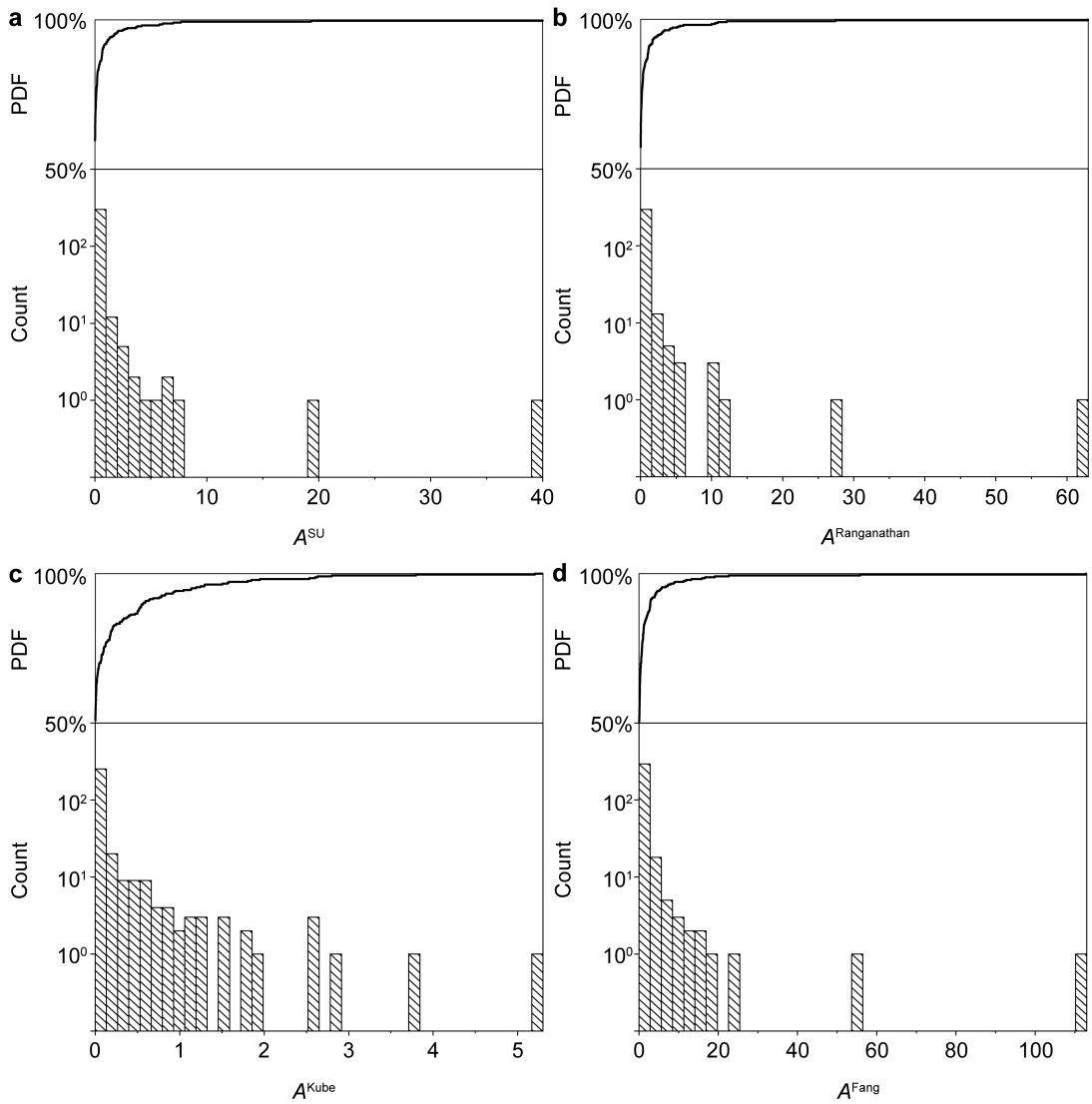

Fig. S1. Probability distribution function (PDF) and statistical distribution of (a) A^{SU}, (b) $A^{\mathrm{Ranganathan}}$, (c) A^{Kube} and (d) A^{Fang}.

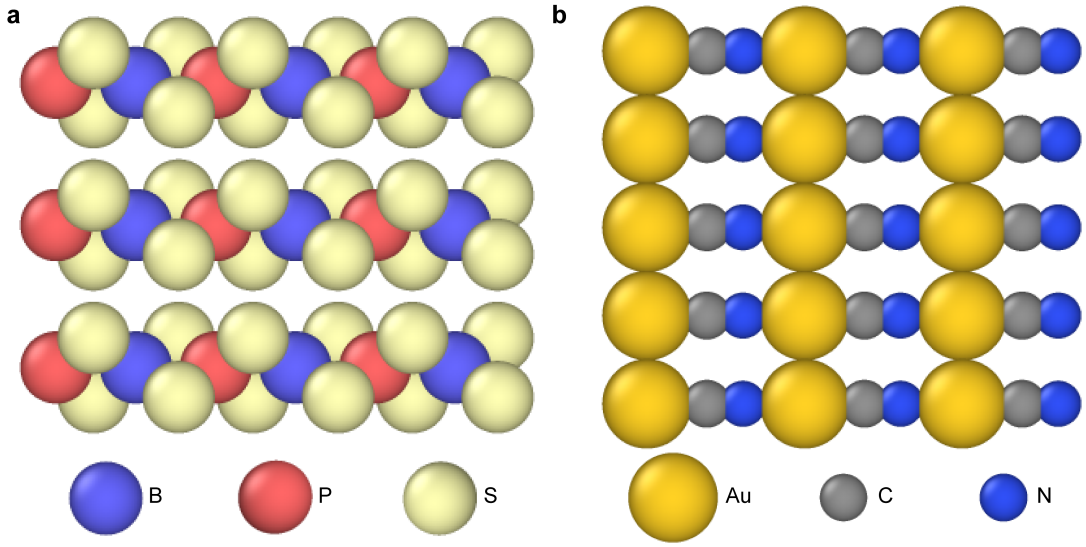

Fig. S2. Top views of the atomic structures of (a) BPS_4 and (b) AuCN.

S4. Supplemental table

Table S1 Details of all the 2D crystals from four lattice systems.

JVASP-ID	Material	Lattice System	A^{SU}	$A^{Ranganathan}$	A^{Kube}	A^{Fang}	K^V/K^R	G^V/G^R
646	NbS_2	Hexagonal	0.00	0.00	0.00	0.00	1.000	1.000
649	$MoSe_2$	Hexagonal	0.00	0.00	0.00	0.00	1.000	1.000
652	WSe_2	Hexagonal	0.00	0.00	0.00	0.00	1.000	1.000
655	$NbSe_2$	Hexagonal	0.00	0.00	0.00	0.01	1.000	1.000
658	WS2	Hexagonal	0.00	0.00	0.00	0.00	1.000	1.000
664	MoS_2	Hexagonal	0.00	0.00	0.00	0.00	1.000	1.000
667	C	Hexagonal	0.00	0.00	0.00	0.00	1.000	1.000
670	Te_2Mo	Hexagonal	0.00	0.00	0.00	0.01	1.000	1.000
687	GaSe	Hexagonal	0.00	0.00	0.00	0.00	1.000	1.000
688	BN	Hexagonal	0.00	0.00	0.00	0.00	1.000	1.000
689	ZrS_2	Hexagonal	0.00	0.00	0.00	0.00	1.000	1.000
696	CrS_2	Hexagonal	0.00	0.00	0.00	0.03	1.000	1.000
705	$HfTe_2$	Hexagonal	0.00	0.00	0.00	0.01	1.000	1.000
728	HfS_2	Hexagonal	0.00	0.00	0.00	0.00	1.000	1.000
729	$HfSe_2$	Hexagonal	0.00	0.00	0.00	0.01	1.000	1.000
735	Te_2Pd	Hexagonal	0.00	0.00	0.00	0.01	1.000	1.000
738	PtO_2	Hexagonal	0.00	0.00	0.00	0.00	1.000	1.000
741	PtS_2	Hexagonal	0.00	0.00	0.00	0.00	1.000	1.000
744	$PtSe_2$	Hexagonal	0.00	0.00	0.00	0.00	1.000	1.000
747	Te_2Pt	Hexagonal	0.00	0.00	0.00	0.01	1.000	1.000
756	SnS_2	Hexagonal	0.00	0.00	0.00	0.00	1.000	1.000
762	$SnSe_2$	Hexagonal	0.00	0.00	0.00	0.00	1.000	1.000
765	TiO_2	Hexagonal	0.00	0.00	0.00	0.00	1.000	1.000
768	Ti_2O	Hexagonal	0.00	0.00	0.00	0.00	1.000	1.000
771	TiS_2	Hexagonal	0.00	0.00	0.00	0.00	1.000	1.000
774	TiS_2	Hexagonal	0.00	0.00	0.00	0.01	1.000	1.000
777	$TiSe_2$	Hexagonal	0.00	0.00	0.00	0.01	1.000	1.000
789	$ZrSe_2$	Hexagonal	0.00	0.00	0.00	0.00	1.000	1.000
5874	PtO_2	Hexagonal	0.00	0.00	0.00	0.00	1.000	1.000
5887	$CdBr_2$	Hexagonal	0.00	0.00	0.00	0.02	1.000	1.000
5905	BCl_3	Hexagonal	0.00	0.00	0.00	0.09	1.000	1.002
5911	$SiTe_2$	Hexagonal	0.00	0.00	0.00	0.00	1.000	1.000
5920	$TaSe_2$	Hexagonal	0.00	0.00	0.00	0.00	1.000	1.000
5932	VS_2	Hexagonal	0.00	0.00	0.00	0.00	1.000	1.000
5944	GaS	Hexagonal	0.00	0.00	0.00	0.00	1.000	1.000
5950	Sc_2C	Hexagonal	0.00	0.00	0.00	0.00	1.000	1.000
5956	$TaSe_2$	Hexagonal	0.00	0.00	0.00	0.00	1.000	1.000
5965	MgI_2	Hexagonal	0.00	0.00	0.00	0.00	1.000	1.000
5968	SbI_3	Hexagonal	0.00	0.00	0.00	0.00	1.000	1.000
5977	$NiTe_2$	Hexagonal	0.00	0.00	0.00	0.01	1.000	1.000
5980	$TaSe_2$	Hexagonal	0.00	0.00	0.00	0.00	1.000	1.000
5986	$MgCl_2$	Hexagonal	0.00	0.00	0.00	0.00	1.000	1.000
5995	PbI_2	Hexagonal	0.00	0.00	0.00	0.00	1.000	1.000
5998	GeI_2	Hexagonal	0.00	0.00	0.00	0.00	1.000	1.000
6013	$TaSe_2$	Hexagonal	0.00	0.00	0.00	0.00	1.000	1.000

6031	MnI_2	Hexagonal	0.00	0.00	0.00	0.01	1.000	1.000
6034	$CoBr_2$	Hexagonal	0.00	0.00	0.00	0.00	1.000	1.000
6037	$ZrCl_2$	Hexagonal	0.00	0.00	0.00	0.00	1.000	1.000
6040	$MgBr_2$	Hexagonal	0.00	0.00	0.00	0.01	1.000	1.000
6052	CaI_2	Hexagonal	0.00	0.00	0.00	0.00	1.000	1.000
6055	$FeCl_2$	Hexagonal	0.00	0.00	0.00	0.01	1.000	1.000
6064	$MnCl_2$	Hexagonal	0.00	0.00	0.00	0.00	1.000	1.000
6067	$MnBr_2$	Hexagonal	0.00	0.00	0.00	0.01	1.000	1.000
6070	TaS_2	Hexagonal	0.00	0.00	0.00	0.00	1.000	1.000
6079	InSe	Hexagonal	0.00	0.00	0.00	0.00	1.000	1.000
6094	BiI_3	Hexagonal	0.00	0.00	0.00	0.03	1.000	1.000
6097	VCl_3	Hexagonal	0.00	0.00	0.00	0.01	1.000	1.000
6106	BI_3	Hexagonal	0.00	0.00	0.00	0.06	1.000	1.001
6142	$ScCl_3$	Hexagonal	0.00	0.00	0.00	0.00	1.000	1.000
6163	BiTeCl	Hexagonal	0.00	0.00	0.00	0.01	1.000	1.000
6172	Sc_2CCl_2	Hexagonal	0.00	0.00	0.00	0.00	1.000	1.000
6199	PI_3	Hexagonal	0.00	0.00	0.00	0.06	1.000	1.001
6229	BiTeI	Hexagonal	0.00	0.00	0.00	0.00	1.000	1.000
6232	$CdCl_2$	Hexagonal	0.00	0.00	0.00	0.01	1.000	1.000
6277	$U(OF)_2$	Hexagonal	0.00	0.00	0.00	0.01	1.000	1.000
6304	$TlSbO_3$	Hexagonal	0.00	0.00	0.00	0.00	1.000	1.000
6313	$AlSiTe_3$	Hexagonal	0.00	0.00	0.00	0.01	1.000	1.000
6427	$TlPd_2Se_3$	Hexagonal	0.00	0.00	0.00	0.00	1.000	1.000
6517	GaN	Hexagonal	0.00	0.00	0.00	0.00	1.000	1.000
6742	$FeCl_3$	Hexagonal	0.00	0.00	0.00	0.01	1.000	1.000
6844	YbSe	Hexagonal	0.00	0.00	0.00	0.00	1.000	1.000
8879	VCl_2	Hexagonal	0.00	0.00	0.00	0.02	1.000	1.000
8912	AsI_3	Hexagonal	0.00	0.00	0.00	0.00	1.000	1.000
8915	$CoCl_2$	Hexagonal	0.00	0.00	0.00	0.01	1.000	1.000
8981	K_4HgAs_2	Hexagonal	0.00	0.00	0.00	0.01	1.000	1.000
8996	Sb_2Te_2Se	Hexagonal	0.00	0.00	0.00	0.00	1.000	1.000
13509	Sb_2TeSe_2	Hexagonal	0.00	0.00	0.00	0.01	1.000	1.000
13528	HoBrO	Hexagonal	0.00	0.00	0.00	0.00	1.000	1.000
13536	SbTe	Hexagonal	0.00	0.00	0.00	0.00	1.000	1.000
13539	Sb	Hexagonal	0.00	0.00	0.00	0.03	1.000	1.000
13546	VBr_2	Hexagonal	0.00	0.00	0.00	0.02	1.000	1.000
13576	$FeBr_2$	Hexagonal	0.00	0.00	0.00	0.00	1.000	1.000
13588	ScHCl	Hexagonal	0.00	0.00	0.00	0.00	1.000	1.000
13632	$TiCl_3$	Hexagonal	0.00	0.00	0.00	0.01	1.000	1.000
14419	CoI_2	Hexagonal	0.00	0.00	0.00	0.01	1.000	1.000
14427	YI_3	Hexagonal	0.00	0.00	0.00	0.02	1.000	1.000
14443	YBrO	Hexagonal	0.00	0.00	0.00	0.00	1.000	1.000
14445	BiOF	Hexagonal	0.00	0.00	0.00	0.00	1.000	1.000
14451	Si_3H	Hexagonal	0.00	0.00	0.00	0.00	1.000	1.000
14456	CoO_2	Hexagonal	0.00	0.00	0.00	0.00	1.000	1.000
14457	VO_2	Hexagonal	0.00	0.00	0.00	0.00	1.000	1.000
14459	BiO_2	Hexagonal	0.00	0.00	0.00	0.03	1.000	1.000
14460	Cr_3O_8	Hexagonal	0.00	0.00	0.00	0.00	1.000	1.000
19510	$NbSe_2$	Hexagonal	0.00	0.00	0.00	0.00	1.000	1.000

19988	AlN	Hexagonal	0.00	0.00	0.00	0.00	1.000	1.000
20002	Bi	Hexagonal	0.00	0.00	0.00	0.00	1.000	1.000
20035	$Rb_3Mo_2Cl_9$	Hexagonal	0.00	0.00	0.00	0.02	1.000	1.000
27724	Sb_2Te_3	Hexagonal	0.00	0.00	0.00	0.01	1.000	1.000
27726	Zr_2Te_2P	Hexagonal	0.00	0.00	0.00	0.00	1.000	1.000
27738	ThI_2	Hexagonal	0.00	0.00	0.00	0.01	1.000	1.000
27754	$Ni(HO)_2$	Hexagonal	0.00	0.00	0.00	0.04	1.000	1.000
27758	HfNCl	Hexagonal	0.00	0.00	0.00	0.00	1.000	1.000
27774	HfIN	Hexagonal	0.00	0.00	0.00	0.00	1.000	1.000
27777	ZrNCl	Hexagonal	0.00	0.00	0.00	0.00	1.000	1.000
27778	Bi_2Pt	Hexagonal	0.00	0.00	0.00	0.03	1.000	1.000
27782	FeI_2	Hexagonal	0.00	0.00	0.00	0.01	1.000	1.000
27862	As	Hexagonal	0.00	0.00	0.00	0.00	1.000	1.000
27864	Ti_2Te_2P	Hexagonal	0.00	0.00	0.00	0.00	1.000	1.000
27872	Ho_2C	Hexagonal	0.00	0.00	0.00	0.00	1.000	1.000
27912	FeO_2	Hexagonal	0.00	0.00	0.00	0.00	1.000	1.000
27913	$Mn(HO)_2$	Hexagonal	0.00	0.00	0.00	0.01	1.000	1.000
27920	NiI_2	Hexagonal	0.00	0.00	0.00	0.04	1.000	1.000
27926	TbCl	Hexagonal	0.00	0.00	0.00	0.01	1.000	1.000
27950	$P_2Pd_3S_8$	Hexagonal	0.00	0.00	0.00	0.00	1.000	1.000
27958	$Mg(HO)_2$	Hexagonal	0.00	0.00	0.00	0.00	1.000	1.000
27999	YCl	Hexagonal	0.00	0.00	0.00	0.00	1.000	1.000
28000	SmSI	Hexagonal	0.00	0.00	0.00	0.00	1.000	1.000
28011	YbClO	Hexagonal	0.00	0.00	0.00	0.00	1.000	1.000
28065	$AgBi(PSe_3)_2$	Hexagonal	0.00	0.00	0.00	0.00	1.000	1.000
28080	$Bi_2Pb_2Se_5$	Hexagonal	0.00	0.00	0.00	0.00	1.000	1.000
28089	Lu_2CCl_2	Hexagonal	0.00	0.00	0.00	0.00	1.000	1.000
28112	$CdInGaS_4$	Hexagonal	0.00	0.00	0.00	0.00	1.000	1.000
28115	TbH_2Br	Hexagonal	0.00	0.00	0.00	0.00	1.000	1.000
28183	$TiSnO_3$	Hexagonal	0.00	0.00	0.00	0.00	1.000	1.000
28223	$Fe(CO_3)_2$	Hexagonal	0.00	0.00	0.00	0.00	1.000	1.000
28277	$B_2(CN_2)_3$	Hexagonal	0.00	0.01	0.00	0.11	1.000	1.003
28291	CoS_2	Hexagonal	0.00	0.00	0.00	0.01	1.000	1.000
28295	NiS_2	Hexagonal	0.00	0.00	0.00	0.00	1.000	1.000
28296	SnO_2	Hexagonal	0.00	0.00	0.00	0.00	1.000	1.000
31357	Nb_3I_8	Hexagonal	0.00	0.00	0.00	0.00	1.000	1.000
31367	ZrBr	Hexagonal	0.00	0.00	0.00	0.01	1.000	1.000
31373	Bi_2Se_3	Hexagonal	0.00	0.00	0.00	0.00	1.000	1.000
31374	ZrBrN	Hexagonal	0.00	0.00	0.00	0.00	1.000	1.000
31420	Te_3As_2	Hexagonal	0.00	0.00	0.00	0.00	1.000	1.000
60279	NbS_2	Hexagonal	0.00	0.00	0.00	0.00	1.000	1.000
60295	Nb_3Br_8	Hexagonal	0.00	0.00	0.00	0.00	1.000	1.000
60332	CeSiI	Hexagonal	0.00	0.00	0.00	0.00	1.000	1.000
60360	BiTeBr	Hexagonal	0.00	0.00	0.00	0.00	1.000	1.000
60385	PbI_2	Hexagonal	0.00	0.00	0.00	0.02	1.000	1.000
60402	YClO	Hexagonal	0.00	0.00	0.00	0.00	1.000	1.000
60416	VS_2	Hexagonal	0.00	0.00	0.00	0.00	1.000	1.000
60442	PbI_2	Hexagonal	0.00	0.00	0.00	0.00	1.000	1.000
60452	GaSe	Hexagonal	0.00	0.00	0.00	0.00	1.000	1.000

60460	BiI_3	Hexagonal	0.00	0.00	0.00	0.00	1.000	1.000
60469	YbI_2	Hexagonal	0.00	0.00	0.00	0.00	1.000	1.000
60495	ZrIN	Hexagonal	0.00	0.00	0.00	0.00	1.000	1.000
60526	PbI_2	Hexagonal	0.00	0.00	0.00	0.00	1.000	1.000
60564	PrBrO	Hexagonal	0.00	0.00	0.00	0.00	1.000	1.000
60566	$MoSe_2$	Hexagonal	0.00	0.00	0.00	0.00	1.000	1.000
60567	$NbSe_2$	Hexagonal	0.00	0.00	0.00	0.00	1.000	1.000
60585	TmClO	Hexagonal	0.00	0.00	0.00	0.00	1.000	1.000
75043	ZrN_2	Hexagonal	0.00	0.00	0.00	0.01	1.000	1.000
75134	$Rb_3Nb_2Br_9$	Hexagonal	0.00	0.00	0.00	0.04	1.000	1.000
75165	SmZnPO	Hexagonal	0.00	0.00	0.00	0.00	1.000	1.000
75287	Y_3I_7O	Hexagonal	0.00	0.00	0.00	0.03	1.000	1.000
75290	YIO	Hexagonal	0.00	0.00	0.00	0.00	1.000	1.000
75293	$HoBiO_3$	Hexagonal	0.00	0.00	0.00	0.00	1.000	1.000
75331	VOF	Hexagonal	0.00	0.00	0.00	0.00	1.000	1.000
75378	Na_2Cl	Hexagonal	0.00	0.00	0.00	0.00	1.000	1.000
6157	PrIO	Square	0.00	0.01	0.00	0.11	1.000	1.003
6241	KMnP	Square	0.00	0.00	0.00	0.09	1.000	1.002
8891	BaIF	Square	0.00	0.00	0.00	0.10	1.000	1.002
8936	SrO_2	Square	0.00	0.00	0.00	0.10	1.000	1.002
9059	RbLiS	Square	0.00	0.01	0.00	0.12	1.000	1.003
13527	NdIO	Square	0.00	0.01	0.00	0.11	1.000	1.003
20033	SmBrO	Square	0.00	0.00	0.00	0.09	1.000	1.002
28095	Pb_2O_3	Square	0.00	0.00	0.00	0.07	1.000	1.001
31348	HfSiTe	Square	0.00	0.00	0.00	0.06	1.000	1.001
60361	UTeN	Square	0.00	0.00	0.00	0.01	1.000	1.000
60413	NpIO	Square	0.00	0.00	0.00	0.06	1.000	1.001
60579	YBrO	Square	0.00	0.01	0.00	0.13	1.000	1.004
75076	HfSiSe	Square	0.00	0.00	0.00	0.03	1.000	1.000
6178	ThIN	Square	0.01	0.01	0.01	0.16	1.000	1.006
6280	ThBrN	Square	0.01	0.02	0.01	0.20	1.000	1.008
8966	ThNCl	Square	0.01	0.01	0.01	0.15	1.000	1.005
9065	RbLiSe	Square	0.01	0.01	0.01	0.13	1.000	1.004
28173	HoIO	Square	0.01	0.02	0.01	0.22	1.000	1.010
60553	YIO	Square	0.01	0.02	0.01	0.20	1.000	1.008
60610	LuBrO	Square	0.01	0.01	0.01	0.14	1.000	1.005
75119	UBrN	Square	0.01	0.01	0.01	0.15	1.000	1.005
75141	UTeO	Square	0.01	0.02	0.01	0.19	1.000	1.008
75385	$AgBiO_2$	Square	0.01	0.02	0.01	0.20	1.000	1.008
6208	SrHI	Square	0.02	0.03	0.02	0.27	1.000	1.014
6214	BiIO	Square	0.02	0.03	0.02	0.27	1.000	1.014
8861	BaO_2	Square	0.02	0.03	0.02	0.30	1.000	1.017
8867	KAgSe	Square	0.02	0.03	0.02	0.26	1.000	1.014
8927	SrHBr	Square	0.02	0.02	0.02	0.25	1.000	1.012
19517	NaMnP	Square	0.02	0.03	0.02	0.27	1.000	1.015
60609	LuIO	Square	0.02	0.03	0.02	0.28	1.000	1.015
13579	SrIF	Square	0.04	0.05	0.03	0.37	1.000	1.025
60289	CaClF	Square	0.04	0.06	0.04	0.42	1.000	1.031
9002	KMgSb	Square	0.05	0.06	0.04	0.43	1.000	1.032

13541	Ta_2Se	Square	0.05	0.07	0.05	0.46	1.000	1.037
6217	BiBrO	Square	0.07	0.09	0.06	0.53	1.000	1.046
6220	BiClO	Square	0.07	0.10	0.07	0.57	1.000	1.052
13590	CaHBr	Square	0.07	0.10	0.07	0.56	1.000	1.050
13589	CaHI	Square	0.10	0.15	0.10	0.71	1.000	1.074
75174	$Sr(ClO_2)_2$	Square	0.11	0.16	0.11	0.75	1.000	1.081
13634	NiSe	Square	0.13	0.18	0.12	0.82	1.000	1.092
19579	Ba_2ZrS_4	Square	0.32	0.46	0.29	1.51	1.000	1.228
19516	SmS	Square	0.38	0.53	0.33	1.69	1.000	1.265
6121	$NdTe_3$	Square	0.43	0.60	0.37	1.86	1.000	1.302
13567	CeS	Square	0.63	0.89	0.52	2.50	1.000	1.446
14431	MnSe	Square	0.80	1.13	0.63	3.00	1.000	1.563
75393	AlP	Square	1.14	1.61	0.84	4.02	1.000	1.806
60433	$ZnWO_4$	Square	1.29	1.82	0.91	4.46	1.000	1.910
75282	Li_2WS_4	Square	1.34	1.90	0.94	4.63	1.000	1.951
786	ZrS	Square	1.73	2.45	1.13	5.75	1.000	2.225
14417	AgI	Square	2.86	4.05	1.57	9.00	1.000	3.025
75380	PbBrCl	Square	3.65	5.17	1.80	11.25	1.000	3.583
27773	$ZnCl_2$	Square	7.68	10.85	2.63	22.67	1.000	6.427
5959	TaS_2	Rectangular	0.00	0.00	0.00	0.00	1.000	1.000
6100	$AlCl_3$	Rectangular	0.00	0.00	0.00	0.01	1.000	1.000
6136	$IrCl_3$	Rectangular	0.00	0.00	0.00	0.01	1.000	1.000
6202	$IrBr_3$	Rectangular	0.00	0.00	0.00	0.02	1.000	1.000
6751	$PbBr_2$	Rectangular	0.00	0.00	0.00	0.06	1.001	1.001
13525	$CaPbI_4$	Rectangular	0.00	0.00	0.00	0.02	1.000	1.000
20014	YCl_3	Rectangular	0.00	0.00	0.00	0.04	1.000	1.000
28013	Tl2O	Rectangular	0.00	0.00	0.00	0.01	1.000	1.000
31379	CoO_2	Rectangular	0.00	0.00	0.00	0.04	1.000	1.000
60264	$TbCl_3$	Rectangular	0.00	0.01	0.00	0.11	1.001	1.003
60552	$CaPbI_4$	Rectangular	0.00	0.00	0.00	0.03	1.000	1.000
6091	PBr_3	Rectangular	0.01	0.01	0.01	0.15	1.005	1.003
6181	TiNCl	Rectangular	0.01	0.01	0.01	0.16	1.000	1.006
6184	TiBrN	Rectangular	0.01	0.01	0.01	0.18	1.001	1.007
6193	InClO	Rectangular	0.01	0.01	0.01	0.14	1.002	1.004
8888	TeRhCl	Rectangular	0.01	0.02	0.01	0.22	1.001	1.010
8948	InBrO	Rectangular	0.01	0.02	0.01	0.18	1.003	1.007
8951	KTlO	Rectangular	0.01	0.01	0.01	0.16	1.001	1.005
13529	ErClO	Rectangular	0.01	0.02	0.01	0.21	1.009	1.006
19513	$P4S_3$	Rectangular	0.01	0.02	0.01	0.18	1.002	1.007
19551	$DyCl_3$	Rectangular	0.01	0.01	0.01	0.12	1.003	1.003
27759	ScBrO	Rectangular	0.01	0.01	0.01	0.15	1.003	1.005
60550	HoBrO	Rectangular	0.01	0.02	0.01	0.22	1.010	1.006
60554	TmClO	Rectangular	0.01	0.02	0.01	0.20	1.009	1.005
60556	TmBrO	Rectangular	0.01	0.02	0.01	0.19	1.008	1.005
75107	KH_2N	Rectangular	0.01	0.02	0.01	0.21	1.000	1.009
14432	$AlHO_2$	Rectangular	0.02	0.04	0.02	0.28	1.013	1.013
6139	PCl_3	Rectangular	0.03	0.04	0.03	0.32	1.001	1.019
6187	AuI	Rectangular	0.03	0.05	0.03	0.36	1.004	1.023
6271	AlClO	Rectangular	0.03	0.04	0.03	0.34	1.000	1.022

27891	ZrIN	Rectangular	0.03	0.05	0.03	0.35	1.004	1.023
60453	HfBrN	Rectangular	0.03	0.04	0.03	0.33	1.000	1.020
68932	WS_2	Rectangular	0.03	0.05	0.03	0.31	1.018	1.015
75219	$BaThBr_6$	Rectangular	0.03	0.06	0.03	0.35	1.020	1.020
661	Te_2W	Rectangular	0.04	0.07	0.04	0.42	1.031	1.018
14421	ZrBrN	Rectangular	0.04	0.06	0.04	0.40	1.003	1.029
75164	$CdBiClO_2$	Rectangular	0.05	0.07	0.04	0.43	1.007	1.032
673	Te_2Mo	Rectangular	0.07	0.13	0.07	0.55	1.039	1.044
28270	BiS_2	Rectangular	0.07	0.12	0.07	0.62	1.060	1.031
676	Te_2Mo	Rectangular	0.08	0.13	0.07	0.56	1.039	1.046
19991	Rb_2Te	Rectangular	0.08	0.13	0.07	0.59	1.055	1.037
75132	InTeBr	Rectangular	0.08	0.12	0.07	0.64	1.062	1.031
6166	DySI	Rectangular	0.09	0.15	0.09	0.65	1.029	1.063
75372	LuH_2ClO_2	Rectangular	0.09	0.15	0.09	0.71	1.073	1.038
723	$PdSe_2$	Rectangular	0.10	0.18	0.10	0.75	1.081	1.047
6073	CaSn	Rectangular	0.10	0.14	0.09	0.67	1.001	1.067
19989	SnS	Rectangular	0.10	0.16	0.10	0.70	1.016	1.072
27841	HoSI	Rectangular	0.10	0.16	0.10	0.68	1.030	1.067
13551	HfS_3	Rectangular	0.12	0.20	0.12	0.79	1.025	1.086
14420	$Nb(SeBr)_2$	Rectangular	0.13	0.19	0.12	0.80	1.014	1.089
75188	LuSBr	Rectangular	0.13	0.22	0.12	0.77	1.062	1.080
6169	DySBr	Rectangular	0.14	0.22	0.13	0.84	1.029	1.095
6205	LuSBr	Rectangular	0.15	0.24	0.14	0.88	1.037	1.102
792	ZrS_3	Rectangular	0.16	0.25	0.15	0.92	1.026	1.110
6145	US_3	Rectangular	0.18	0.26	0.17	1.01	1.012	1.126
6196	ErSCl	Rectangular	0.18	0.28	0.17	1.01	1.033	1.126
60357	VBrO	Rectangular	0.18	0.29	0.17	1.12	1.148	1.073
75397	$CaTlCl_3$	Rectangular	0.18	0.26	0.17	1.02	1.003	1.128
6175	ErSeI	Rectangular	0.19	0.32	0.18	1.04	1.061	1.130
19539	Te_2AuCl	Rectangular	0.19	0.32	0.18	0.98	1.110	1.106
27870	$HfSe_3$	Rectangular	0.19	0.28	0.18	1.03	1.013	1.131
75209	Ca_3SiBr_2	Rectangular	0.20	0.34	0.19	1.02	1.101	1.119
6151	TiS_3	Rectangular	0.21	0.33	0.20	1.13	1.033	1.150
75387	$LiCuO_2$	Rectangular	0.21	0.33	0.19	1.10	1.044	1.143
19549	$LiBiO_2$	Rectangular	0.22	0.37	0.20	1.14	1.152	1.110
28028	$NbIO_2$	Rectangular	0.22	0.32	0.21	1.16	1.004	1.156
6019	$ZrSe_3$	Rectangular	0.23	0.33	0.21	1.19	1.012	1.161
75319	$LiVF_3$	Rectangular	0.25	0.43	0.24	1.24	1.095	1.167
6328	KAuS	Rectangular	0.32	0.55	0.29	1.41	1.189	1.179
6340	RbAuS	Rectangular	0.34	0.60	0.31	1.49	1.203	1.197
27756	AuBr	Rectangular	0.36	0.51	0.32	1.64	1.000	1.254
60293	PdI_2	Rectangular	0.38	0.62	0.34	1.83	1.295	1.164
20054	PS	Rectangular	0.46	0.65	0.40	1.96	1.001	1.324
19576	$CaCO_3$	Rectangular	0.48	0.76	0.42	2.01	1.089	1.334
28280	$AgBiO_2$	Rectangular	0.56	0.83	0.47	2.26	1.051	1.391
75382	$HAuO_2$	Rectangular	0.58	1.00	0.50	2.18	1.345	1.326
6118	TiI_3	Rectangular	0.59	0.99	0.50	2.31	1.197	1.395
60320	$Sr(BiO_2)_2$	Rectangular	0.60	0.97	0.50	2.70	1.493	1.237
75185	$CdBiS_2Cl$	Rectangular	0.61	0.99	0.51	2.76	1.506	1.243

75124	SrH_4O_3	Rectangular	0.64	1.03	0.53	2.85	1.527	1.252
5983	P	Rectangular	0.65	1.08	0.54	2.83	1.522	1.277
13602	PtI_2	Rectangular	0.65	1.09	0.55	2.69	1.490	1.301
60235	P	Rectangular	0.65	1.07	0.54	2.82	1.520	1.276
6058	Te_2Br	Rectangular	0.68	1.13	0.56	2.87	1.532	1.297
8972	$KAuSe_2$	Rectangular	0.72	1.21	0.59	2.89	1.537	1.337
60403	$SrBiBrO_2$	Rectangular	0.73	1.06	0.59	2.81	1.026	1.519
75175	$AgBiSCl_2$	Rectangular	0.81	1.31	0.65	3.41	1.659	1.328
6361	SbSeI	Rectangular	0.84	1.45	0.68	2.95	1.421	1.515
31349	As	Rectangular	0.95	1.64	0.76	3.24	1.585	1.529
6082	Te_2I	Rectangular	1.03	1.66	0.78	4.26	1.864	1.398
19552	Br_2O	Rectangular	1.03	1.66	0.78	4.26	1.862	1.399
27847	SiS	Rectangular	1.12	1.66	0.83	3.95	1.086	1.788
13596	AuSe	Rectangular	1.22	2.12	0.93	3.98	1.698	1.710
75099	I	Rectangular	1.53	2.33	1.04	5.13	1.186	2.072
27885	GeS	Rectangular	1.66	2.75	1.14	5.37	1.528	2.112
6223	$OsCl_2O$	Rectangular	1.76	2.94	1.19	5.62	1.606	2.167
28311	SbN	Rectangular	2.01	3.31	1.30	7.34	2.614	1.850
20022	RbI_3	Rectangular	2.08	3.15	1.29	6.71	1.238	2.458
31418	$SbAsO_4$	Rectangular	2.64	4.46	1.58	7.96	2.041	2.712
6016	SiS_2	Rectangular	5.75	9.96	2.53	15.89	4.365	4.299
6265	$AlPS_4$	Rectangular	6.05	10.48	2.60	16.68	4.402	4.539
6190	BPS_4	Rectangular	6.99	12.11	2.80	19.11	5.072	5.017
20029	AuCN	Rectangular	39.99	62.95	5.21	112.74	8.360	28.797
75146	$AlBiBr_6$	Oblique	0.07	0.11	0.06	0.55	1.025	1.042
13611	PI_2	Oblique	0.10	0.18	0.10	0.77	1.075	1.050
60262	Bi_2O_3	Oblique	0.19	0.33	0.18	1.20	1.134	1.099
60607	$Al2Te_5$	Oblique	0.19	0.31	0.18	1.16	1.155	1.079
75135	$LiAuI_4$	Oblique	0.23	0.40	0.22	1.23	1.137	1.131
60251	InSe	Oblique	0.28	0.39	0.25	1.35	1.000	1.195
6115	AlI_3	Oblique	0.44	0.74	0.39	2.10	1.169	1.286
75254	$TlInS_2$	Oblique	0.62	0.96	0.52	2.68	1.092	1.433
60548	$HgPSe_3$	Oblique	0.67	1.17	0.57	2.61	1.418	1.374
75078	Tl_2SiSe_3	Oblique	1.93	3.05	1.24	7.20	1.370	2.341
31361	$Pd(Se_3Cl)_2$	Oblique	2.46	4.13	1.50	8.76	1.884	2.624
75265	Ag_3SI	Oblique	3.78	5.52	1.85	11.87	1.176	3.670
19557	$Pt(SCl_3)_2$	Oblique	4.18	6.03	1.95	13.19	1.116	3.957
19996	KCN	Oblique	19.30	27.39	3.80	55.82	1.094	14.649